

Implementation of angular response function modeling in SPECT simulations with GATE

This article has been downloaded from IOPscience. Please scroll down to see the full text article.

2010 Phys. Med. Biol. 55 N253

(<http://iopscience.iop.org/0031-9155/55/9/N04>)

View [the table of contents for this issue](#), or go to the [journal homepage](#) for more

Download details:

IP Address: 132.166.112.37

The article was downloaded on 19/07/2011 at 11:16

Please note that [terms and conditions apply](#).

NOTE

Implementation of angular response function modeling in SPECT simulations with GATE

P Descourt¹, T Carlier^{2,3}, Y Du⁴, X Song⁴, I Buvat⁵, E C Frey⁴,
M Bardies², B M W Tsui⁴ and D Visvikis¹

¹ INSERM, U650, LaTIM, IFR SclnBioS; Université de Brest; CHU Brest; Brest, F-29200, France

² CRCNA INSERM U892, Nantes, France

³ Service de Médecine Nucléaire, Centre Hospitalier Universitaire, Nantes, France

⁴ Department of Radiology, J Hopkins University, Baltimore, MD, USA

⁵ IMNC-UMR 8165 CNRS Universités Paris 7 et Paris 11, Orsay, France

E-mail: dimitris@univ-brest.fr

Received 1 November 2009, in final form 11 March 2010

Published 14 April 2010

Online at stacks.iop.org/PMB/55/N253

Abstract

Among Monte Carlo simulation codes in medical imaging, the GATE simulation platform is widely used today given its flexibility and accuracy, despite long run times, which in SPECT simulations are mostly spent in tracking photons through the collimators. In this work, a tabulated model of the collimator/detector response was implemented within the GATE framework to significantly reduce the simulation times in SPECT. This implementation uses the angular response function (ARF) model. The performance of the implemented ARF approach has been compared to standard SPECT GATE simulations in terms of the ARF tables' accuracy, overall SPECT system performance and run times. Considering the simulation of the Siemens Symbia T SPECT system using high-energy collimators, differences of less than 1% were measured between the ARF-based and the standard GATE-based simulations, while considering the same noise level in the projections, acceleration factors of up to 180 were obtained when simulating a planar 364 keV source seen with the same SPECT system. The ARF-based and the standard GATE simulation results also agreed very well when considering a four-head SPECT simulation of a realistic Jaszczak phantom filled with iodine-131, with a resulting acceleration factor of 100. In conclusion, the implementation of an ARF-based model of collimator/detector response for SPECT simulations within GATE significantly reduces the simulation run times without compromising accuracy.

1. Introduction

Monte Carlo (MC) simulations play an important role in medical imaging and radiotherapy (Zaidi 1999, Rogers 2006, Visvikis *et al* 2006, Verhaegen and Seuntjens 2003). In medical

imaging, simulations are primarily used for the design and optimization of new and existing imaging devices, and for the assessment of acquisition and processing protocols. Among the MC codes available for simulations in emission tomography (Buvat and Castiglioni 2002), GATE, the Geant4 Toolkit for Emission Tomography, is a powerful, reliable and versatile tool for simulating PET and SPECT scans (Jan *et al* 2004). However, GATE simulations are often lengthy. One of the most significant reasons is the low efficiency of Geant4 for tracking photons in a geometry described as a large set of voxels. This limitation has been recently tackled by implementing fictitious interactions in GATE (Rehfeld *et al* 2009), or by separating the phantom and detector parts of the simulation, either within GATE (Descourt and Visvikis 2008) or combining GATE with SimSET/PHG so that the latter manages the photon tracking in the voxelized phantom before the propagation results are fed to GATE which manages the detector and associated electronics modeling (Chen *et al* 2008). A second reason for the long simulation times is the precise modeling of the collimator in SPECT, where photon tracking in the collimator is extremely time consuming. Because parallel hole collimators are composed of thousands of holes, the photon tracking accounting for septal penetration and interactions, such as Compton scattering, photo-electric absorption and x-ray fluorescence, is computationally very demanding. For realistic parallel hole collimators, roughly one 140 keV photon over 640 entering the collimator is detected for a low-energy high-resolution collimator (148 000 holes for a 53×39 cm² surface) in a 15% energy window and only one 364 keV photon over 1550 for a high-energy collimator (8000 holes for a 53×39 cm² surface). Yet, the precise modeling of the collimator/detector response is essential for accurate simulations of SPECT datasets, especially when septal penetration and scattering in the collimator are prominent (Dewaraja *et al* 2000, Rault *et al* 2007). For example collimator scatter could account for as much as 30% of the detected counts in a 20% window around 364 keV (Dewaraja *et al* 2000) for I-131 imaging. In this note, we address this specific issue of computationally demanding particle tracking in the collimator within the GATE MC simulation platform.

One approach to tackle this problem consists in using a tabulated modeling of the collimator/detector response instead of tracking each particle in the collimator. Early work regarding the tabulation of the detector point spread function (PSF) was proposed for the Utrecht Monte Carlo System (Beekman *et al* 1999). This idea was next incorporated in various MC codes using the concept of convolution-based forced detection (CFD) and validated for ^{99m}Tc (de Jong *et al* 2001, Liu *et al* 2008, De Beenhouwer *et al* 2008). However, these methods did not consider the septal penetration component, given that septal penetration can be neglected for the low-energy photons (140 keV) of ^{99m}Tc. More recently, a fast method was developed for incorporating the effects of septal penetrating photons and was validated for ²⁰¹Tl and ¹¹¹In (Staelens *et al* 2007), showing a reduction in computation time by up to four orders of magnitude associated with small accuracy losses (7% and 8% for ²⁰¹Tl and ¹¹¹In, respectively, considering an optimum, in terms of accuracy loss and speed improvement, object voxelization and detector pixelization). This approach has not been assessed in the context of ¹³¹I and the use of high-energy collimators.

The method presented in this work and implemented in GATE is also based on the use of tabulated responses, namely angular response functions (ARF) (Frey and Tsui 2006). The ARF is a function of energy and direction of the incident photon. It represents the probability that a photon hitting the surface of the collimator will either interact with or pass through the collimator and be detected, with an energy included in a given energy range, at the intersection point of the photon direction vector and the detection plane. These functions once tabulated and computed for a given collimator/detector pair and energy window, may be subsequently used for any simulation involving this specific collimator/detector pair. Like in CFD, the use

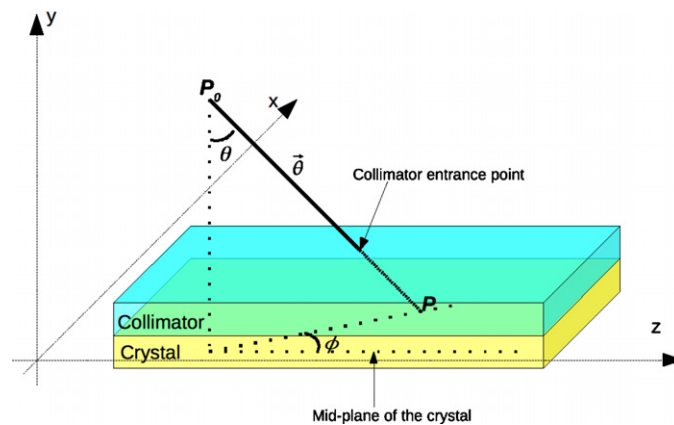


Figure 1. Angular parameterization of the ARF method. P_0 is the emission point. P is the geometric point of intersection of the photon, defined as the intersection of the line with direction θ considering the mid-plane of the crystal.

of these functions removes the need for tracking the photons inside the collimator/detector volumes, which in turn yields significant reductions in run time.

In the implementation described here, an integrated solution is proposed in the sense that GATE manages both the generation of the ARF tables and their use in subsequent simulations. The model accuracy and associated run times are assessed for the elementary SPECT system used in the GATE SPECT benchmark and for a realistic clinical SPECT system.

2. Materials and methods

2.1. Angular response function

The angular response function refers to the spatial distribution of photons detected for a given point source position. It is related to the collimator/detector response function (CDRF) which is the image generated from a point source. The ARF is a function of the polar angle θ and azimuthal angle ϕ of incidence of a photon with respect to the collimator surface (figure 1), the incident energy, the energy window of interest and the energy resolution of the system.

The CDRF is the primary factor determining the image resolution in SPECT (Frey and Tsui 2006). It represents the probability that photons emitted at some point in space will be detected at a given position on the detection plane. This CDRF can be decomposed into four components: (1) the intrinsic response function (response of the scintillation camera without any collimator to a pencil beam of radiation), (2) the geometric response function (response to detected photons which travel through the collimator holes without interaction), (3) the septal penetration response function (response to photons which go through the collimator septa) and (4) the septal scatter response function (response to photons which scatter in the collimator septa).

As described in Song *et al* (2005), a key approximation of the ARF model is that a photon interacting with the collimator can be assumed to be detected at the geometric intersection point defined as the point where the incident photon direction vector intersects the detection plane usually taken halfway through the crystal thickness. The ARF should actually also depend on

the position of the incidence of the photon relative to the collimator surface. However, when the collimator septal thickness is small compared to the intrinsic resolution (including pixel size effects), the CDRF may be approximated as being spatially invariant over the collimator unit cell.

The value of the ARF table normalized to an incident photon for a given solid angle (θ, ϕ) is given by

$$P(\theta, \phi) = \frac{N_{\text{counts}}(E_{\text{in}}, R, E_T, E_u, \theta, \phi)}{N(\theta, \phi)} \quad (1)$$

where E_{in} is the photon incident energy, R is the detector energy resolution and the range $[E_T, E_u]$ defines the energy window of interest. The numerator N_{counts} is the contribution of all the photons which deposit energy in the infinitesimal solid angle $\Delta\Omega(\theta, \phi)$ and the denominator N denotes the number of photons whose incidence vector is located within this same solid angle $\Delta\Omega(\theta, \phi)$. If N_0 denotes the total number of simulated photons in a 4π steradian solid angle, we have

$$N(\theta, \phi) = \frac{\Delta\Omega(\theta, \phi)}{4\pi} N_0. \quad (2)$$

2.2. ARF table computation within GATE

The strategy used in Song *et al* (2005) for the implementation of the ARF approach took advantage of the SIMSET/PHG simulation code to generate the list mode files from which the ARF tables were deduced using external programs. In our implementation, the data needed for calculating the ARF tables are produced with GATE and used within GATE to derive the CDRF tables. New C++ classes have been designed to handle all tasks with versatile GATE script commands that allow the user to generate and compute the tables (Descourt *et al* 2008). This new development is publicly available since the GATE version 5.0.0. The ARF computation process can be divided into two separate steps as are described below.

First, photons are emitted from a rectangular source in air within a given incident energy window. The source to collimator distance was set to 34 cm. This distance was chosen so that the rectangular source covered several holes to average out the effects of the collimator hole pattern (Song *et al* 2005). The photons undergoing photoelectric absorption in the crystal (after Compton interactions or not) are collected, and the deposited energy and corresponding incidence angles with respect to the collimator plane are stored into ROOT files (<http://root.cern.ch/drupal>).

In the second step, the collected data are used to generate the ARF table for a given incident energy or a small incident energy window. This ARF table is computed for a given energy resolution and energy window of interest. In this work, two different ARF tables were calculated for comparison purposes.

- The raw ARF table (denoted by ARF_r) is directly computed from equations (1) and (2),
- In addition to the solid angle binning used for the ARF_r , the emission point coordinates are subtracted from the detection point coordinates. The detected photons are subsequently binned on the detection plane to derive the CDRF. For each solid angle bin, the averaged sum in the CDRF table of all the bins inside a disk with a fixed radius is computed. The ARF tables are then deduced from the CDRF. These ARF tables are denoted as ‘averaged tables’ (ARF_a).

Table 1. Characteristics of the two SPECT systems simulated in this work.

SPECT system	Benchmark SPECT (scripted within GATE)	Clinical system (Siemens Symbia T)
Collimator		
Number of hexagonal parallel holes	18 000	8000
Hole length (mm)	30	59.7
Hole inner radius (mm)	1.5	2
Septal thickness (mm)	0.6	2
Transverse dimension (cm ²)	19 × 28	57 × 44
NaI(Tl) crystal thickness (mm)	10	9.5

2.3. Sampling of ARF tables

The ARF tables were calculated considering photons with energy between 364 and 365 keV for the simulations involving only a monoenergetic source of 364 keV. In this case, 10 billion photons were simulated to compute each of the ARF tables (one for the SPECT benchmark set-up and one for the clinical system, described in section 2.4 below). When considering simulations in a scattering medium for the iodine-131 source with several emission energies (364.5 keV, 637 keV and 723 keV for the main photopeaks), a set of 44 ARF_a tables were computed. The spectrum of iodine-131 was sampled in 10 keV wide energy intervals from 304 to 364 keV (6 intervals), 365 to 635 keV (27 intervals) and 639 to 709 keV (7 intervals). Three additional tables were computed for the three main emission photopeaks (ranges: 364–365 keV, 635–639 keV and 722–723 keV for the 364 keV, 637 keV and 723 keV, respectively). The last ARF table covered the range from 709 to 722 keV. Five billion up to 80 billion photons were simulated in 4π steradians for the simulation of each ARF table.

2.4. Validation

Two detector models were considered. The first was the hypothetical detector used in the SPECT benchmark provided with the GATE distribution (GATE user's guide, www.opengatecollaboration.org). The second was a model of the Siemens Symbia T system (Carlier *et al* 2008) equipped with a high-energy collimator. The main properties of these two systems are summarized in table 1. For both setups, all images were 128×128 (pixel size: 4.8×4.8 mm²).

A point source was first simulated in air. Profiles across the point sources were drawn for visual comparison of the standard (sGATE) and ARF-based (ARF–GATE) GATE simulations. A root mean squared difference index (RMSD) was also calculated to measure the agreement between sGATE and ARF–GATE using

$$\text{RMSD}(\text{ARF}, \text{sGATE}) = \sqrt{\frac{1}{N} \sum_{k=1}^N (B_k^{\text{ARF}} - B_k^{\text{sGATE}})^2} \quad (3)$$

where B_k^{ARF} is the content of voxel k in ARF-simulated images (B_k^{sGATE} is for the sGATE simulated images, respectively). For RMSD calculation, the images were first normalized to 1.0 and the computation was performed only for pixel values greater than 0.1.

A uniform planar source (30×30 cm²) was also simulated in air with all photons forced in the solid angle of the detector plane. Profiles through the sGATE and ARF–GATE images were drawn, and RMSD was calculated. The acceleration factor resulting from ARF–GATE

was computed considering the same statistical quality between ARF-GATE and sGATE simulations. The statistical quality was defined as the standard deviation divided by the mean over a region of interest (ROI) including at least 400 pixels within the image of the uniform source.

The clinical SPECT system sensitivity (counts $\text{MBq}^{-1} \text{s}^{-1}$) was derived based on ten simulations (16 s each) of a point source (3 MBq in 4π sr). The count density in the images was computed and normalized by the activity and the time. Mean and standard deviations of total count density were derived from the ten independent simulations.

For the point source and planar source simulations, 364 keV photons were simulated to assess the use of ARF-GATE for simulations involving a monoenergetic source in air and a 15% energy window around 364 keV was considered for detection.

The computational efficiency was also estimated for a realistic Jaszczak phantom (diameter: 21.6 cm; length: 18.6 cm) uniformly filled with iodine-131 and centered in the field of view. SPECT simulations involving four heads of the Siemens Symbia T system with 64 projections (16 steps per head; projection matrix size: $64 \times 64 \times 64$; pixel size: $9.6 \times 9.6 \text{ mm}^2$) were performed using sGATE and ARF-GATE. The simulation results were compared by calculating the RMSD for the two sets of 64 projections. The acceleration factor was calculated when reaching the same noise level in the projections for the two simulations. The noise level was calculated first in each projection, as the standard deviation divided by the mean over a region of interest (ROI) including at least 400 pixels and then averaged over all projections. This noise level is not intended to be a reliable measurement of noise partly because of the spatially dependent attenuation effect but rather as an index of comparison between two datasets corresponding to the same set-up.

3. Results

For the GATE SPECT benchmark, the ARF tables are shown in figure 2. The averaged table, ARF_a (figure 2(B)), is computed from the smooth CDRF (figure 3(A)). The hole effect pattern seen in figure 3(B) is removed in ARF_a (figure 2(B)). The ARF_r and ARF_a tables computed for the clinical SPECT camera are shown in figure 4.

The ARF profile for the 0° polar angle is shown in figure 2 for the GATE SPECT benchmark and in figure 4 for the clinical SPECT camera. The noisy nature of the ARF_r table compared to the ARF_a tables is clearly demonstrated, as well as the 'wavy' behavior at a low azimuthal angle induced by the hole pattern effect. This effect at low incidence angles may come from the septal thickness that modifies the CRDF by introducing the honeycomb structure from the collimator hexagonal holes (see figure 3(B)).

Figure 5 shows the projections obtained using the GATE SPECT benchmark and the clinical SPECT system for the point source simulations using the ARF_r , ARF_a tables and sGATE simulations. The ARF-GATE and sGATE projections agreed well. The RMSD averaged over the 64 projections were 0.02 for the SPECT benchmark and 0.09 for the clinical SPECT system when comparing sGATE and ARF_r . The RMSD were also 0.02 for the SPECT benchmark and 0.09 for the clinical SPECT system when comparing sGATE and ARF_a . As negligible differences were found between ARF-GATE simulations performed with either ARF_r or ARF_a tables in terms of both visual and quantitative agreements, all subsequent ARF-GATE simulations used the ARF_a table.

The images and x -axis profiles of the uniform source are presented in figure 6 for the SPECT benchmark and clinical SPECT systems. The RMSD for this emission geometry were 0.02 and 0.09 for the SPECT benchmark and clinical SPECT system, respectively. An RMSD of 0.09 was also found when repeating two independent sGATE simulations for the

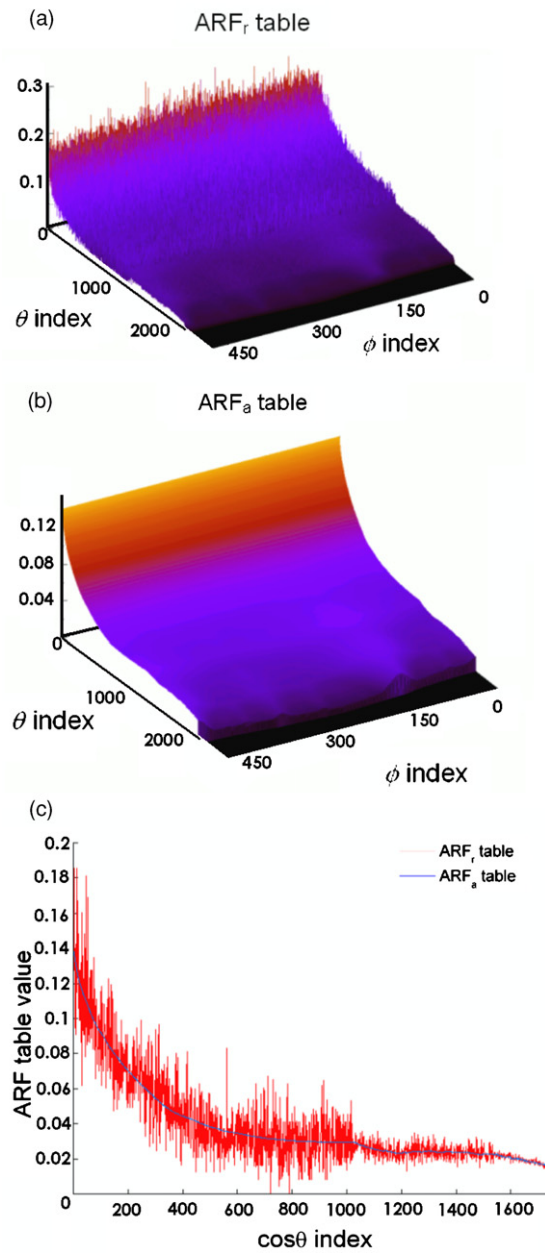


Figure 2. 2D ARF tables derived for the GATE benchmark SPECT system. (A) Raw ARF table, ARF_r ; (B) averaged ARF table, ARF_a ; (C) ARF profiles for a 0° polar angle: ARF_r versus ARF_a table for the GATE SPECT benchmark. The x -axis units are for the parameterization of $\cos\theta$ ($\cos\theta$ ranges from 0 to 1 and is binned in 2048 bins).

clinical SPECT system, suggesting that there are equivalent differences between two sGATE simulations and that obtained between an sGATE and an ARF-GATE simulation and that the observed RMSD is mostly due to statistical fluctuations.

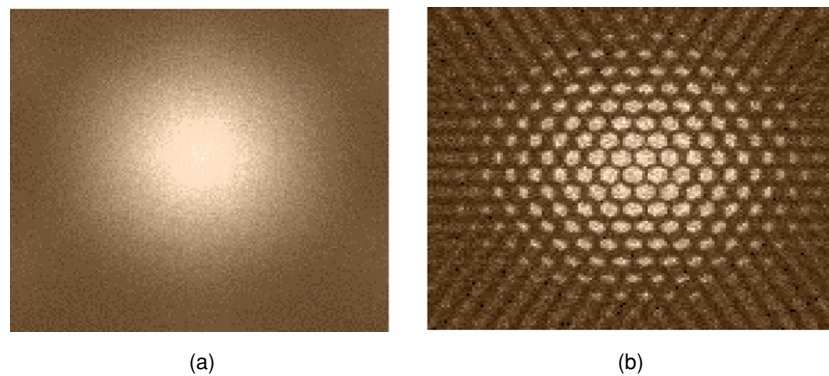


Figure 3. Hole effect pattern on the collimator/detector response function (CDRF). Right: raw CDRF image, left: smoothed CDRF image.

Table 2. Computational efficiency for the GATE benchmark SPECT and clinical SPECT system simulations.

		sGATE	ARF-GATE	Noise level (%)
GATE SPECT benchmark	Number of photon for one run of simulation	5 millions	5 millions	3.8
	Duration time for one run	1148 s	1058 s	
	Number of runs to achieve the same noise level	10	1	
	Total duration time	11 220 s	922 s	
	Speed-up factor		12	
Clinical SPECT system	Number of photon for one run of simulation	20 millions	20 millions	9.8
	Duration time for one run	7520 s	1590 s	
	Number of runs to achieve the same noise level	38	1	
	Total duration time	285 760 s	1590 s	
	Speed-up factor		180	

Fifty million emitted photons were used in the simulation of the sGATE image of the uniform source for the SPECT benchmark simulation, and 7.6 million photons were detected in the 15% energy window. For the simulation of the uniform source in combination with the simulated clinical SPECT system, 760 million photons were emitted in the sGATE simulation and 0.5 million were detected in the 15% energy window. The sGATE simulation took approximately 11 000 s (2.6 GHz Intel core 2 duo) for the SPECT benchmark and 286 000 s for the Siemens Symbia (dual 2.5 GHz PowerPC G5). To achieve the same noise level in the simulated projections (table 2) as when using sGATE, only 5 million and 20 million photons were needed with the ARF-GATE simulation for the SPECT benchmark and the Siemens Symbia SPECT systems, respectively, corresponding to run times of 922 s and 1590 s, respectively, on the same computer specifications. The acceleration factors between ARF-GATE and sGATE were thus approximately 12 for the SPECT benchmark and 180 for the Siemens Symbia SPECT simulations. The same noise level could be reached with 10 and

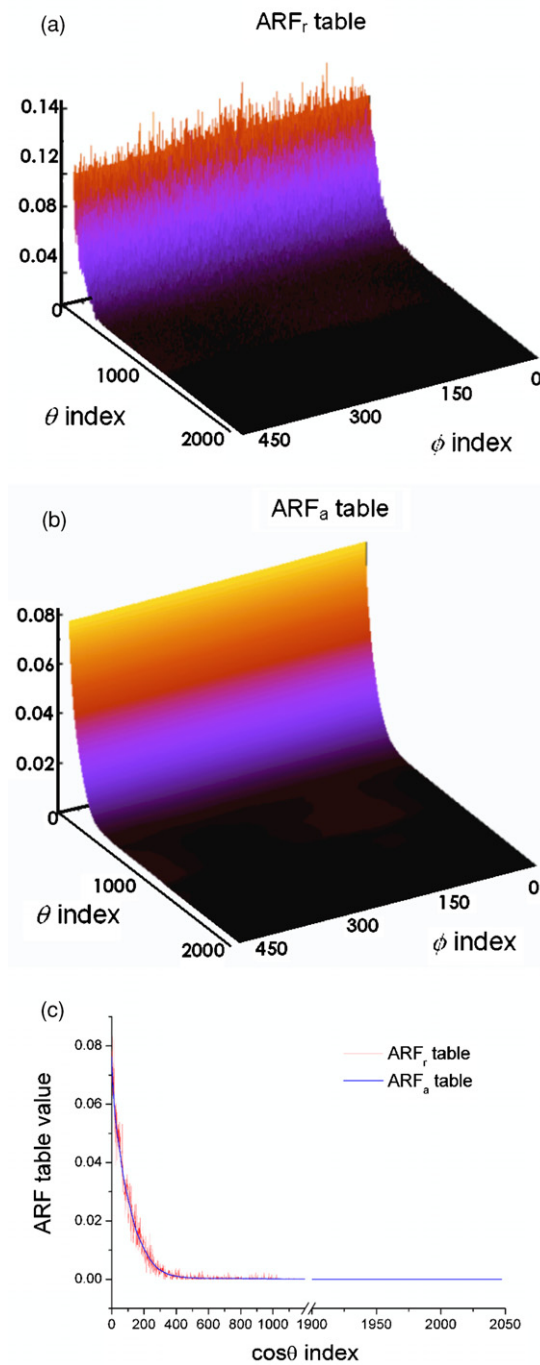


Figure 4. ARF tables generated for the high-energy collimator of the SIEMENS Symbia T clinical SPECT system when considering 364 keV emitted photons. (A) ARF_r table. (B) ARF_a table. (C) ARF profiles for a 0° polar angle: ARF_r versus ARF_a table for the clinical SPECT system. The x -axis units are for the parameterization of $\cos\theta$ ($\cos\theta$ ranges from 0 to 1 and is binned in 2048 bins but only the first 750).

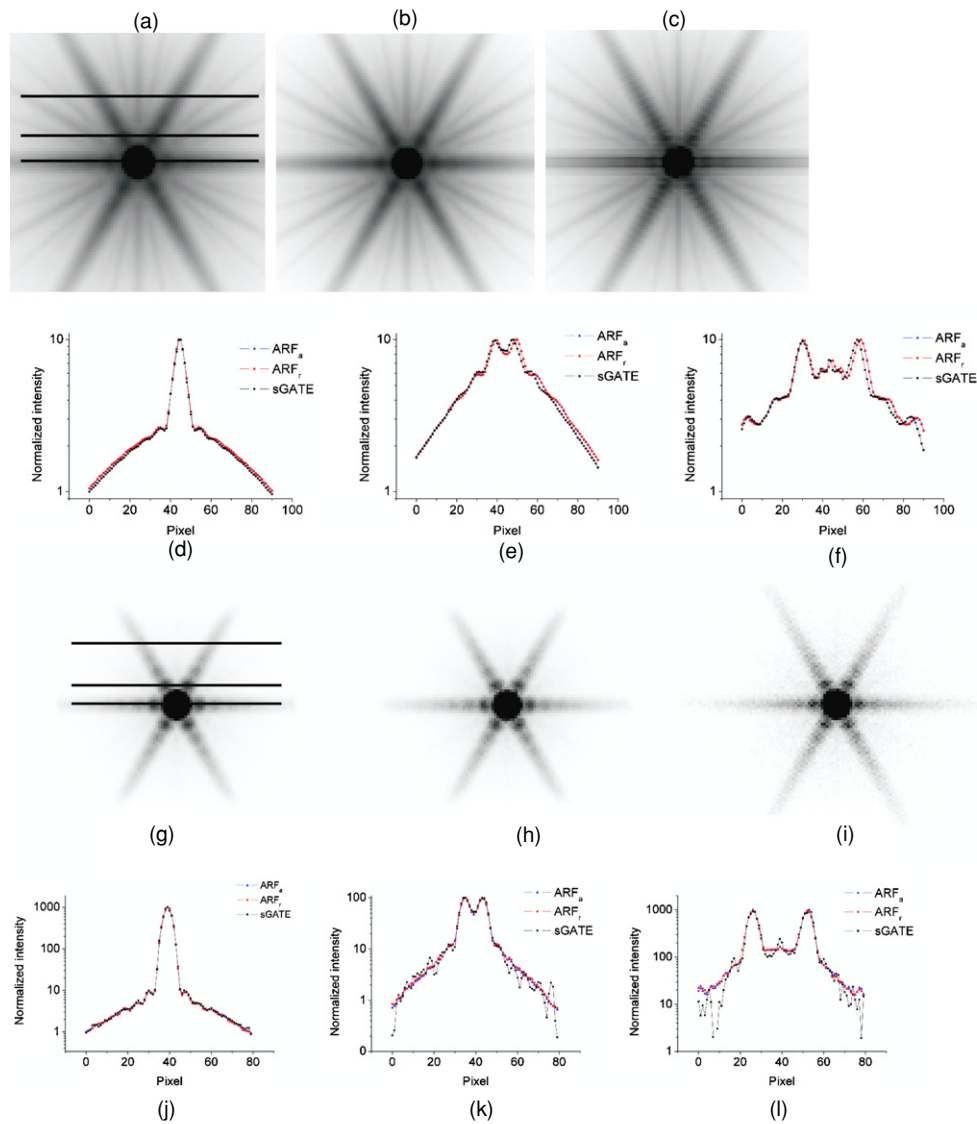


Figure 5. Projection images of a 364 keV point source in air for the collimator/detector of the GATE SPECT benchmark (A), (B) and (C), and the SIEMENS Symbia T SPECT system (G), (H) and (I). The image contrast was enhanced to highlight the common star structure. (A), (G) Images computed with the ARF_a table. (B), (H) Images computed with the ARF_r table. (C), (I) Images computed with sGATE. X-axis profile for ARF-GATE computed using the ARF_r table (red), the ARF_a table (blue) and sGATE (black) for the GATE SPECT benchmark (D), (E) and (F), and the SIEMENS Symbia T SPECT system (J), (K) and (L). The line profiles are drawn in black on the ARF_a projection for the GATE SPECT benchmark and the SIEMENS Symbia T SPECT system.

38 times less photons for the SPECT benchmark and the Siemens Symbia SPECT systems simulations, respectively, when ARF-GATE was used (table 2). The speed-up factor obtained when comparing ARF-GATE with sGATE for the tracking of photons inside the collimator only was also calculated based on a single simulation run considering the clinical SPECT

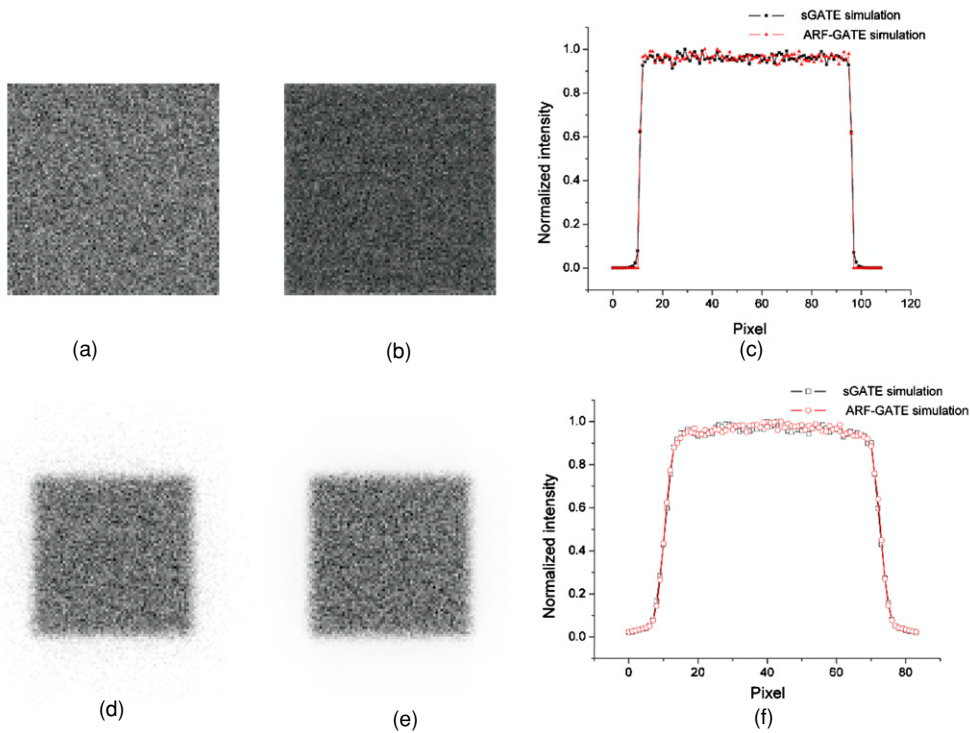


Figure 6. Simulation of the uniform source with 364 keV photons for the GATE SPECT benchmark (A) and (B), and the SIEMENS Symbia T SPECT system (D) and (E). (A), (D) sGATE images of the uniform source. (B), (E) ARF-GATE images of the uniform source. (C), (F) Profiles for ARF-GATE and sGATE.

system (table 2). In this case, the ARF approach lead to an acceleration factor of 11 for a same number of photons reaching the collimator.

The overall system sensitivity was similar for the ARF-GATE (41.9 ± 1.5 counts $\text{MBq}^{-1} \text{s}^{-1}$) and sGATE (41.8 ± 1.8 counts $\text{MBq}^{-1} \text{s}^{-1}$) simulations for the clinical SPECT system.

The complete SPECT simulation of the Jaszczak phantom with sGATE took 33 400 CPU hours. The same simulation with ARF-GATE took 341 CPU hours for the same level of noise in the projections, corresponding to an $\sim \times 100$ acceleration. With the use of ARF-GATE, the same image quality could be reached with 38 times less photons. The profiles of one projection for sGATE and ARF-GATE are shown in figure 7.

4. Discussion

This note describes the validation and evaluation of the implementation of the ARF modeling within the GATE simulation platform. The use of ARF tables within GATE is straightforward. First, the ROOT files produced by the simulation of a rectangular source with the model of the SPECT system of interest are stored. Second, the ARF tables are computed for a given energy window either using equation (1) or based on the computation of the averaged CDRF table.

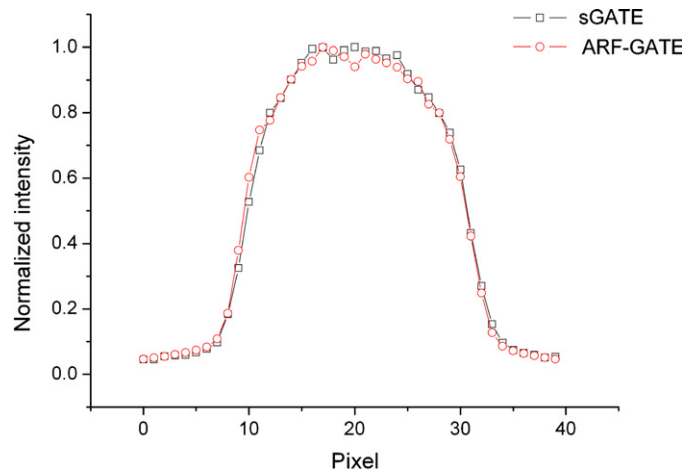


Figure 7. Profiles through a projection for the SPECT simulation of the Jaszczak phantom using ARF-GATE and sGATE.

The use of the averaged ARF tables reduced the local fluctuations introduced by the hole pattern at low azimuthal angles. No RMSD differences were found between the use of the raw and the averaged ARF tables for the simulation of the point source. This is because in the regions of the highest signal ($>10\%$ of the maximum value), the high uncertainties affecting the ARF values of the raw ARF table cancel out given that many photons are detected in these regions. No significant differences were found when comparing ARF-based GATE simulations and those using standard collimator/detector photon tracking for the two detection systems considered here (the hypothetical detector of the GATE SPECT benchmark and the Symbia T camera). This suggests that even for challenging acquisition conditions where septal penetration is high (like in the SPECT benchmark, where 364 keV photons are acquired with the low-energy high-resolution collimator), the results obtained using ARF-GATE simulations are consistent with those of the sGATE simulation. However, as it could be noted in figures 5(D)–(F) and 6(D) and (E), the projections computed with ARF-GATE tend to be more blurred than the one computed with sGATE. This is a direct consequence of the use of the ARF table without the effect of the hole pattern (figure 3(A)). In this case, the pixel size ($4.8 \times 4.8 \text{ mm}^2$) is of the same order of magnitude as the collimator hole diameter (4 mm for the clinical SPECT system considered). As the hole pattern is removed when using the ARF approach, the pixelized behavior of the projection due to the similarity between the pixel size and the collimator hole diameter is also removed compared with the projections simulated with sGATE.

The acceleration factors achieved with ARF-GATE were dependent on the type of collimator used, with a larger impact for the high-energy collimators associated with a larger number of photon interactions within the collimator. The computational efficiency increased by more than two orders of magnitude when ARF-GATE was used for 364 keV photons in air. In a more realistic situation, when considering the complete iodine-131 spectrum in a scattering medium, in combination with a camera equipped with a realistic high-energy collimator, a speed-up factor of ~ 100 was observed. This acceleration factor cannot be readily compared with those reported in Song *et al* (2005), which were derived only based on a visual comparison of the noise texture in the projection images. The comparison of acceleration factors and accuracy with those achieved using other acceleration methods such as CFD is

also difficult as almost no study deals with iodine-131. A recent work of Khosravi *et al* (2007) using the CFD methodology with iodine-131 showed a speed-up factor of roughly 10 without loss of accuracy when comparing with simulation including forced detection only, but this work does not include any detailed report regarding the validation of the simulated collimator response compared to real collimator response.

A major approximation involved in the ARF method is the assumption that the septal thickness is small compared to the intrinsic resolution (including the pixel size effect). For the clinical SPECT system considered here, the ratio of the intrinsic resolution to the septal thickness is 2.5 (and 10 for the GATE SPECT benchmark) compared to 5 for the medium energy collimator of the GE Millennium VG SPECT previously used by Song *et al* (2005). However, the low intrinsic resolution to septal thickness ratio did not have a significant effect on the quantitative results. A ratio of 2.5 could thus be considered as sufficient to compute reliable ARF tables for high-energy collimators.

5. Conclusions

The ARF model for SPECT simulations was implemented within GATE. This implementation reduces the computation time by a factor between 10 and 100, through a decrease of both the time needed to transport the photons and the number of photon decays necessary to obtain a given noise level in the simulated projections.

Acknowledgments

This work was supported by the Cancéropôle Grand Ouest (contract R05014NG) and the French National Research Agency (ANR) (ANR-06-CIS6-004-03).

References

- Beekman F J, de Jong H W A M and Slijpen E T P 1999 Efficient SPECT scatter calculation in non-uniform media using correlated Monte Carlo simulation *Phys. Med. Biol.* **44** N183–92
- Buvat I and Castiglioni I 2002 Monte Carlo simulations in SPET and PET *Q. J. Nucl. Med.* **46** 48–61
- Carlier T, Moisan M, Ferrer L, Kraeber-Bodéré F, Barbet J and Bardies M 2008 Validation of a GATE model of the Siemens Symbia system for ^{99m}Tc , ^{111}In and ^{131}I acquisitions *J. Nucl. Med.* **49** 404P
- Chen C L, Wang Y, Lee J J and Tsui B M W 2008 Integration of SimSET photon history generator in GATE for efficient Monte Carlo simulations of pinhole SPECT *Med. Phys.* **35** 3278–84
- De Beenhouwer J, Staelens S, Vandenberghe S and Lemahieu I 2008 Acceleration of GATE SPECT simulations *Med. Phys.* **35** 1476–85
- de Jong H W A M, Slijpen E T P and Beekman F J 2001 Acceleration of Monte Carlo SPECT simulation using convolution-based forced detection *IEEE Trans. Nucl. Sci.* **48** 58–74
- Descourt P, Du Y, Song X, Frey E C, Tsui B M W and Visvikis D 2008 Angular response function parameterization for collimator/detector in SPECT simulations within the GATE toolkit *IEEE NSS-MIC Conf. Rec.* pp 4969–71
- Descourt P and Visvikis D 2008 Acceleration techniques for new detector architecture simulations *J. Nucl. Med.* **49** 405P
- Dewaraja Y K, Ljungberg M and Koral K F 2000 Characterization of scatter and penetration using Monte Carlo simulation in ^{131}I imaging *J. Nucl. Med.* **41** 123–30
- Frey E C and Tsui B M W 2006 *Quantitative Analysis in Nuclear Medicine Imaging* ed H Zaidi (Berlin: Springer) pp 141–66
- Jan S *et al* 2004 GATE: a simulation toolkit for PET and SPECT *Phys. Med. Biol.* **49** 4543–61
- Khosravi H R, Sarkar S, Takavar A, Saghari M and Shahriari M 2007 Planar and SPECT Monte Carlo acceleration using a variance reduction technique in ^{131}I imaging *Iran. J. Radiat. Res.* **4** 175–82
- Liu S, King M A, Brill A B, Stabin M G and Farncombe T H 2008 Accelerated SPECT Monte Carlo simulation using multiple projection sampling and convolution-based forced detection *IEEE Trans. Nucl. Sci.* **55** 560–7

- Rault E, Vandenberghe S, Van Holen R, De Beenhouwer J, Staelens S and Lemahieu I 2007 Comparison of image quality of different iodine isotopes (I-123, I-124 and I-131) *Cancer Biother. Radiopharm.* **22** 423–30
- Rehfeld N S, Stute S, Apostolakis J, Soret M and Buvat I 2009 Introducing improved voxel navigation and fictitious interaction tracking in GATE for enhanced efficiency *Phys. Med. Biol.* **54** 2163–78
- Rogers D W 2006 Fifty years of Monte Carlo simulations for medical physics *Phys. Med. Biol.* **51** R287–301
- Song X, Segars W P, Du Y, Tsui B M W and Frey E C 2005 Fast modelling of collimator-detector response in Monte Carlo simulation of SPECT imaging using the angular response function *Phys. Med. Biol.* **50** 1791–804
- Staelens S, de Wit T and Beekman F 2007 Fast hybrid SPECT simulation including efficient septal penetration modeling (SP-PSF) *Phys. Med. Biol.* **52** 3027–43
- Verhaegen F and Seuntjens J 2003 Monte Carlo modelling of external radiotherapy photon beams *Phys. Med. Biol.* **48** R107–64
- Visvikis D, Bardies M, Chiavassa S, Danford C, Kirov A, Lamare F, Maigne L, Staelens S and Taschereau R 2006 Use of the GATE Monte Carlo package for dosimetry applications *Nucl. Instrum. Methods A* **569** 335–40
- Zaidi H 1999 Relevance of accurate Monte Carlo modeling in nuclear medical imaging *Med. Phys.* **26** 574–608